A new hyperelastic strain energy function and integrity basis of invariants for modelling transversely isotropic materials

Renye Cai, Frédéric Holweck, Zhi-Qiang Feng, François Peyraut

A new hyperelastic strain energy function and integrity basis of invariants for modelling transversely isotropic materials

Renye Cai [a], Frédéric Holweck [b], Zhi-Qiang Feng [c, d], François Peyraut [b]

[a] *School of Automobile and Transportation Engineering, Guangdong Polytechnic Normal University, Guangdong, China*

[b] *ICB, UMR 6303, CNRS, Université Bourgogne Franche-Comté, UTBM, F-90010 Belfort, France*

[c] *School of Mechanics and Engineering, Southwest Jiaotong University, Chengdu, China*

[d] *LMEE Univ-Evry, Université Paris-Saclay, 91020 Evry, France*

Abstract – The present paper proposes a new Strain Energy Function (SEF) for incompressible transversely isotropic hyperelastic materials, i.e. materials with a single fiber family. This SEF combines polyconvex invariants forming an integrity basis [1] in a polynomial and exponential form. Compared to a previous attempt for building a SEF based on the same invariants [2], we have reduced the number of material parameters from 23 to 10, without losing any accuracy on the numerical results. The 10 material parameters are identified by comparing the closed form solutions deriving from our model with experimental and numerical data extracted from the literature. These data concern uniaxial tension and shear tests, both parallel and transverse to the fiber direction [3, 4], as well as shear calculations with 9 different fiber angles [5]. Due to the variety of the considered situations, we have developed specific identification strategies based on: 1) the linear or nonlinear nature of the material parameters of the model; 2) the modeling of the free boundary conditions by a spectral approach.

Keywords: Transversely isotropic hyperelastic materials, Strain Energy Function (SEF), Biological soft tissue, Polyconvexity, Large deformation, Nonlinear calculation.

1. Introduction

Understanding the behavior of transversely isotropic hyperelastic materials is a keystone for scientists because their modeling has a wide range of applications in engineering science and health therapeutic, like medical prosthesis, ergonomics and manufacturing. For example, virtual surgery simulation could obtain a realistic rendering of biological soft tissue behavior, which is helpful for surgical planning and treatment [6]. It is accepted that these materials are anisotropic due to the embedded fiber and that their mechanical behavior can be modelled through an appropriate SEF [7].

These past twenty years, many SEF have been proposed for transversely isotropic materials to investigate the mechanical behavior of biological soft tissues [8]. Shearer [9] built for example a SEF for the hyperelastic modeling of ligaments and tendons based on the geometrical arrangement of their fibrils. Limbert et al. [10] proposed a phenomenological constitutive law to describe the anisotropic visco-hyperelastic behavior of the human posterior cruciate ligament at high strain rates. For the fiber-reinforced rubber materials, Ciarletta et al. [3] introduced a new hyperelastic model using a non-classical measure of strains. In the same vein, Fereidoonnezhad et al. [11] built later a model using this kind of strains, reporting the nonlinearity aspect from the form of the SEF to the strain invariant. All these models, like most of the papers published in the literature, divide the SEF into an isotropic part and an anisotropic part. The first part is used to model the low strain behavior of the ground matrix and the second part accounts for the behavior of the fibers at higher strain [12, 13]. A first alternative to this standard method is to replace scalar-invariant based approach by operations between fourth-order tensors [14]. Another alternative consists in using an integrity basis of invariants as proposed in [1], and mixing them in a single SEF [2]. This second alternative, mathematically justified by the theory of invariant polynomials and by Noether's theorem, is inspired by the pioneering work of Thionnet et al. [15]. The polyconvexity and physical sense of the invariants forming the integrity basis exhibited in [1] are discussed in [2]. In addition, the attempt made in [2] for building a SEF combining these invariants with polynomial and power form functions provided an excellent correlation with experimental data. However, two drawbacks can be reported:

1) a large number of material parameters (up to 23) making the physical interpretation of these parameters difficult,

2) some convergence problem at low strain due to the logarithmic singularity near zero of power form functions.

To overcome these two drawbacks, we propose in Section 3 of this paper a new SEF combining the same invariants as the ones used in [2], but with an exponential function with respect to these invariants, instead of a power form one. An exponential function actually offers a perfect regularity, contrarily to a power form function, avoiding any convergence problems. In addition, without losing any accuracy on the numerical results, we have simplified the SEF by reducing the number of material parameters from 23 to 10. Considering some specific loadings, it is possible to reduce more the number of material parameters. For example, we prove in section 4.1 that our model can be reduced from 10 to 5 material parameters in the case of a uniaxial tensile loading. In section 5.4, we also demonstrate that our model can be reduced from 10 to 7 material parameters in the case of a shear loading. However, in the most complicated loading cases, if for example tensile and shear tests are both accounted, the use of the 10 material parameters embedded in our model is required. As we aimed to develop a model capable of encompassing as many cases as possible, instead of a model dealing with a single application, we keep all the 10 material parameters. Anisotropic hyperelasticity is a dynamic field of research and many models are proposed in the literature. But, contrarily to isotropic hyperelasticity, a few receives a full consensus, except perhaps the well-known HGO model [8] to name a few. It is therefore useful to propose a general model covering a wide range of applications and efficient in as many cases as possible.

The 10 material parameters embedded in our model are identified in Section 5 by comparing closed form solutions (Section 4) with experimental and numerical data extracted from the literature. These data concern uniaxial tension and shear tests, both parallel and transverse to the fiber direction [3, 4], as well as shear calculations with 9 different fiber angles [5]. The most complicated case to fit concerns the experimental data extracted from [3]. As reported in [11], it is difficult to match these data by using standard models such as the ones introduced in [24-26]. To the best of our knowledge, there are few models in the literature attempting to match these data, except those proposed in [3] and [11] which use non classical measure of strain and provide satisfactory predictions with only 4 material

parameters. However, these models use a case sensitive material parameter introducing possible discontinuities in the stress tensor when the fibers change from a tension to a compression state. The model proposed in this paper contains more parameters (10 against 4) but ensures the stress continuity.

Due to the variety of the considered situations, we have developed in Section 5.1 specific identification strategies based on: 1) the linear or nonlinear nature of the material parameters of the model; 2) the modeling of the free boundary conditions by a spectral approach. These strategies have been implemented in the Octave free software [16].

Notations

A bold-face Latin lowercase letter, say $\boldsymbol{a}$, and a bold-face Latin capital letter, say $\boldsymbol{A}$, will denote a vector and second-order tensor, respectively. The standard Euclidean inner product in a *n* vector space dimension, and its related norm, are defined by:

$$< \boldsymbol{A}\boldsymbol{a}, \boldsymbol{a} >= \sum_{i=1}^{n} A_{ij} a_j a_i \;\; ; \;\; \|\boldsymbol{a}\| = \sqrt{\sum_{i=1}^{n} (a_i)^2}$$

The product between two vectors $\boldsymbol{a}$ and $\boldsymbol{b}$, and between two tensors $\boldsymbol{A}$ and $\boldsymbol{B}$ are respectively defined by:

$$(\boldsymbol{a} \otimes \boldsymbol{b})_{ij} = a_i b_j \;\; ; \;\; (\boldsymbol{A} \otimes \boldsymbol{B})_{ijkl} = A_{ij} B_{kl}$$

2. Preliminaries

2.1. Kinematics and basic continuum mechanics

Consider a continuum body $\boldsymbol{V}$ with particle $P \in \boldsymbol{V}$ which is embedded in the three-dimensional Euclidean space at given instant of time *t*. As the continuum body $\boldsymbol{V}$ moves in space from one instant of time to another it occupies a continuous sequence of geometrical regions denoted by $\Omega_0 \ldots \Omega_i$. Ω_0 is referred to as the fixed reference (undeformed or Lagrangian) configuration $(t = 0)$ of the body $\boldsymbol{V}$ while the configuration *t* is called the current (deformed or Eulerian) configuration. The position $\boldsymbol{x}$ of particle *P* in the current (or deformed) configuration can be deduced by the motion φ that depends on its initial position vector $\boldsymbol{X}$ and the time t:

$$\boldsymbol{x} = \varphi(\boldsymbol{X}, t) \tag{1}$$

The transformation gradient tensor $\boldsymbol{F}$ is defined by:

$$\boldsymbol{F} = \frac{\partial \boldsymbol{x}}{\partial \boldsymbol{X}} = \boldsymbol{I} + \frac{\partial \boldsymbol{U}(\boldsymbol{X},t)}{\partial \boldsymbol{X}} \tag{2}$$

where $\boldsymbol{I}$ is the unity tensor and $\boldsymbol{U}(\boldsymbol{X},t) = \boldsymbol{x} - \boldsymbol{X}$ is the displacement vector of the particle. The tensor $\boldsymbol{C}$ is the so-called right Cauchy-Green strain tensor:

$$\boldsymbol{C} = \boldsymbol{F}^T\boldsymbol{F} \tag{3}$$

In terms of stress tensor, we remind that the second Piola-Kirchhoff stress tensor $\boldsymbol{S}$ and the corresponding Cauchy stress tensor $\boldsymbol{\sigma}$ are obtained by differentiating a SEF *W* with respect to $\boldsymbol{C}$:

$$\boldsymbol{S} = 2\frac{\partial W}{\partial \boldsymbol{C}} - p\boldsymbol{C}^{-1} \tag{4}$$

$$\boldsymbol{\sigma} = J^{-1}\boldsymbol{F}\boldsymbol{S}\boldsymbol{F}^T \tag{5}$$

where the extra pressure p is included in the formulation to account for the incompressibility condition $J = \det(\boldsymbol{F}) = 1$. Replacing Eq. (4) into Eq. (5) leads to:

$$\boldsymbol{\sigma} = 2J^{-1}\boldsymbol{F}\frac{\partial W}{\partial \boldsymbol{C}}\boldsymbol{F}^T - p\boldsymbol{I} \tag{6}$$

The so-called first Piola-Kirchhoff stress tensor $\sum$, and the nominal stress $\boldsymbol{P}$, are deduced from Eq. (6) by:

$$\sum = J\boldsymbol{\sigma}\boldsymbol{F}^{-T} = 2\boldsymbol{F}\frac{\partial W}{\partial \boldsymbol{C}} - p\boldsymbol{F}^{-T} \;\; ; \;\; \boldsymbol{P} = \sum^T = J\boldsymbol{F}^{-1}\boldsymbol{\sigma} = 2\frac{\partial W}{\partial \boldsymbol{C}}\boldsymbol{F}^T - p\boldsymbol{F}^{-1} \tag{7}$$

Note that, in the following, the time t will be omitted because we will only deal with static problems.

2.2. Invariants and strain energy functions

In this paper, we focus on a fiber-reinforced material with one fiber family of direction $\boldsymbol{a}$ as depicted on Figure 1. We assume that $\boldsymbol{a}$ lies in the plane $(\boldsymbol{E}_1, \boldsymbol{E}_2)$, forms an angle $\theta \in \left[0, \frac{\pi}{2}\right]$ with $\boldsymbol{E}_1$, and that $\boldsymbol{b}$ is a perpendicular vector to $\boldsymbol{a}$ in the plane $(\boldsymbol{E}_1, \boldsymbol{E}_2)$:

$$\boldsymbol{a} = \begin{pmatrix} c \\ s \\ 0 \end{pmatrix} \;\; ; \;\; \boldsymbol{b} = \begin{pmatrix} -s \\ c \\ 0 \end{pmatrix} \quad \text{with } c = cos(\theta),\ s = sin(\theta) \tag{8}$$

The vector $\boldsymbol{c}$ is defined as the cross product between $\boldsymbol{a}$ and $\boldsymbol{b}$ in order to form a direct orthogonal coordinate system $(\boldsymbol{a}, \boldsymbol{b}, \boldsymbol{c})$:

$$\boldsymbol{c} = \boldsymbol{a} \wedge \boldsymbol{b} = \begin{pmatrix} 0 \\ 0 \\ 1 \end{pmatrix} \tag{9}$$

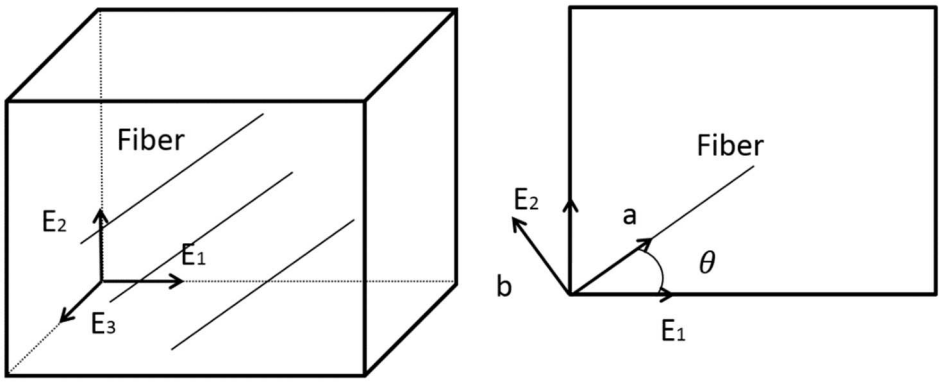

Figure 1 – *A fiber-reinforced material with one-fiber family*

In [1], Ta et al. have introduced a set of five invariant polynomials related to $\boldsymbol{C}$ and forming an integrity basis of the ring of invariant polynomials under the action of the material symmetry group *G*. The introduction of these invariants was based on the concepts of the Noether's theorem, but with an extension of the classical Reynolds operator in order to account for the infinite cardinality of *G*. The polyconvexity of these invariants, noted below K_i, is discussed in [2]. They are defined with respect to six coefficients ρ_i related to the strain tensor $\boldsymbol{C}$:

$$\begin{cases} K_1 = \rho_1 \ ; \ K_2 = \rho_2 + \rho_3 \ ; \ K_3 = \rho_4^2 + \rho_5^2 \ ; \ K_4 = \rho_6^2 - \rho_2\rho_3 \\ K_6 = (\rho_4^2 - \rho_5^2)(\rho_2 - \rho_3) + 4\rho_4\rho_5\rho_6 \end{cases} \tag{10}$$

$$\begin{cases} \rho_1 = \langle \boldsymbol{Ca}, \boldsymbol{a} \rangle \ ; \ \rho_2 = \langle \boldsymbol{Cb}, \boldsymbol{b} \rangle \ ; \ \rho_3 = \langle \boldsymbol{Cc}, \boldsymbol{c} \rangle \\ \rho_4 = \langle \boldsymbol{Ca}, \boldsymbol{b} \rangle \ ; \ \rho_5 = \langle \boldsymbol{Ca}, \boldsymbol{c} \rangle \ ; \ \rho_6 = \langle \boldsymbol{Cb}, \boldsymbol{c} \rangle \end{cases} \tag{11}$$

A SEF *W* being generally defined as a function of $\boldsymbol{C}$ or of its invariants, we assume that $W(K_1, K_2, K_3, K_4, K_6)$. The nominal stress $\boldsymbol{P}$ in the equation (7) can therefore be written as:

$$\boldsymbol{P} = 2\sum_{i=1, i\neq 5}^{6} \omega_i \frac{\partial K_i}{\partial \boldsymbol{C}} \boldsymbol{F}^T - p\boldsymbol{F}^{-1} \tag{12}$$

Where ω_i represent the derivatives of *W* with respect to K_i:

$$\omega_i = \frac{\partial W}{\partial K_i} \tag{13}$$

The derivatives $\frac{\partial K_i}{\partial \boldsymbol{C}}$ are calculated straightforwardly from Eqs. (10) and (11):

$$\begin{cases} \dfrac{\partial K_1}{\partial \boldsymbol{C}} = \boldsymbol{M}_a \quad ; \quad \dfrac{\partial K_2}{\partial \boldsymbol{C}} = \boldsymbol{M}_b + \boldsymbol{M}_c = \boldsymbol{I} - \boldsymbol{M}_a \\ \dfrac{\partial K_3}{\partial \boldsymbol{C}} = 2\rho_4 \boldsymbol{M}_{ab} + 2\rho_5 \boldsymbol{M}_c \; ; \; \dfrac{\partial K_4}{\partial \boldsymbol{C}} = 2\rho_6 \boldsymbol{M}_{bc} - \rho_2 \boldsymbol{M}_c - \rho_3 \boldsymbol{M}_b \\ \dfrac{\partial K_6}{\partial \boldsymbol{C}} = 2(\rho_4 \boldsymbol{M}_{ab} + \rho_5 \boldsymbol{M}_{ac})(\rho_2 - \rho_3) + (\rho_4^2 - \rho_5^2)(\boldsymbol{M}_b - \boldsymbol{M}_c) \\ \qquad +4(\rho_4\rho_5 \boldsymbol{M}_{bc} + \rho_4\rho_6 \boldsymbol{M}_{ac} + \rho_5\rho_6 \boldsymbol{M}_{ab}) \end{cases} \tag{14}$$

where the symmetric matrix $\boldsymbol{M}_a$, $\boldsymbol{M}_b$, $\boldsymbol{M}_c$, $\boldsymbol{M}_{ab}$, $\boldsymbol{M}_{ac}$ and $\boldsymbol{M}_{bc}$ are defined by:

$$\begin{cases} \boldsymbol{M}_a = \boldsymbol{a} \otimes \mathbf{a} \; ; \quad \boldsymbol{M}_b = \boldsymbol{b} \otimes \boldsymbol{b} \; ; \; \boldsymbol{M}_c = \boldsymbol{c} \otimes \boldsymbol{c} \; ; \; \boldsymbol{M}_{ab} = \frac{1}{2}(\boldsymbol{a} \otimes \boldsymbol{b} + \boldsymbol{b} \otimes \boldsymbol{a}) \\ \boldsymbol{M}_{ac} = \frac{1}{2}(\boldsymbol{a} \otimes \boldsymbol{c} + \boldsymbol{c} \otimes \boldsymbol{a}) \; ; \; \boldsymbol{M}_{bc} = \frac{1}{2}(\boldsymbol{b} \otimes \boldsymbol{c} + \boldsymbol{c} \otimes \boldsymbol{b}) \end{cases} \tag{15}$$

To use Eqs. (12)-(13) later, it is necessary to express how W depends on K_i. This issue is discussed in the next section.

3. Material model

Cai et al. [2] have introduced various SEF combining the invariants defined by (10) in a polynomial and in a power law form. However, among these various SEF, the one providing the best fitting with experimental data involves up to 23 material parameters. In order to provide easier-to-use SEF, it is necessary to work with less material parameters. The simplification from the baseline model was performed by trying to match properly the experimental data extracted from [3] because it was the most complicated fitting case we met. It is for example observed in Figure 2 that it is mandatory for a model to provide a linear behavior for matching appropriately the two shear loadings applied parallel and transverse to the fiber direction in the range of moderate deformation of the experimental data extracted from [3].

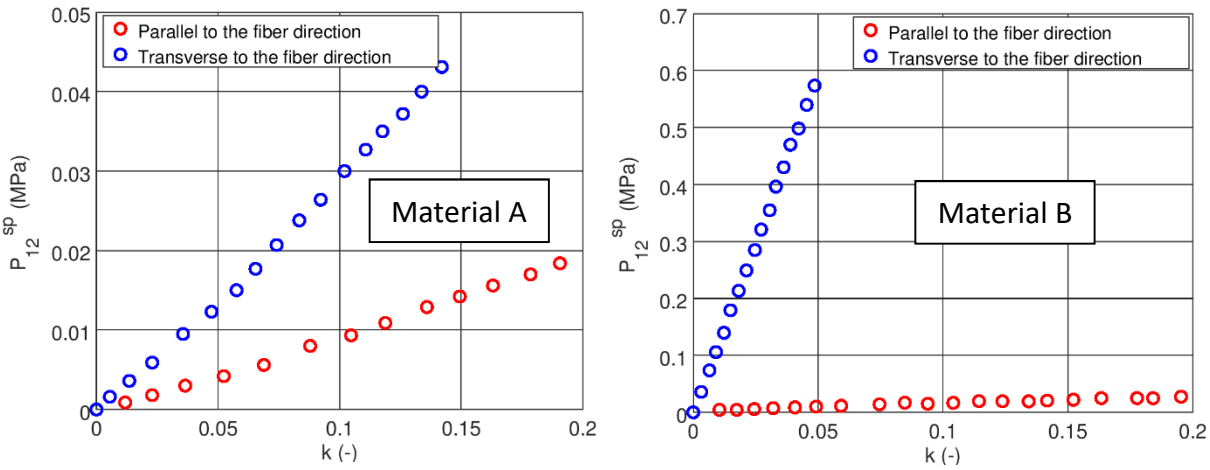

Figure 2 – *Simple shear loading applied parallel and transverse to the fiber direction – Nominal shear stress vs. the amount of shear deformation [3]*

According to the experimental results presented in Figure 2, two conditions must be held:

Condition 1: the dependence of the shear stress with respect to the shear strain must be linear in the range of moderate deformation of the experimental data,

Condition 2: the slopes of the linear dependence must be different if the shear loading is applied parallel or transverse to the fiber direction.

By using these two conditions as a guideline for building a model simpler than the baseline model introduced in [2], we have tested many combinations with the smallest number of parameters as possible. The best model we succeeded to build combines the following polynomial expansion with a case-sensitive function W_{add}:

$$W = \frac{1}{2}\left\{a_2(K_2-2)^2 + a_3{K_3}^2 + a_4(K_4+1)^2\right\} + a_{24}(K_2-2)(K_4+1) + b_3K_3 + b_6K_6 + b_{24}(K_2+K_4-1) + W_{add} \quad (16)$$

$$W_{add} = \begin{cases} \frac{1}{2}\{a_1(K_1-1)^2 + \alpha K_3(exp[\beta(K_1-1)^2]-1)\} & \text{if } K_1 \geq 1 \\ 0 \end{cases} \quad (17)$$

The number of material parameters is thus reduced to 10. This new SEF offers many other advantages:

1. The invariants used to build the SEF form an integrity basis, as reported in [1], and their polyconvex properties were discussed in [2]. In addition, it is possible to attribute a physical sense to them, as demonstrated in [2]: 1) K_1 represents the elongation squared in the fiber direction; 2) K_2 is the elongation squared in the isotropic plane perpendicular to the fiber direction; 3) K_3 is linked to the total amount of shear strain between the fiber direction and the isotropic plane; 4) $-K_4$ is the deformation of an area element with a unit normal parallel to the fiber direction; 5) K_6 is related to the along-fiber shear effect between two adjacent fibers and to the shear interaction between the matrix and the

fiber.

2. Since K_1 represents the elongation squared in the fiber direction, the case-sensitive part (17) of the SEF indicates that a compressive state of the material (K_1<1) does not produce any stress. This observation is consistent with the literature [13].
3. Since K_1 represents the elongation squared in the fiber direction and K_3 the total amount of shear strain between the fiber direction and the isotropic plane, the additional SEF W_{add} mixes tension and shear effects through the product of $exp[\beta(K_1-1)^2]$ by K_3. This property will be useful for identifying the material parameters when both uniaxial tension and simple shear tests will be considered in Section 5.
4. The exponential growth included in the case-sensitive part of the SEF is suitable for capturing the large deformations generally occurring with hyperelastic materials [17, 18].
5. An exponential function can be differentiated as many times as desired, without any restrictions. This property is interesting for planning later a finite element implementation.
6. As it will proved in further sections 5.2 to 5.4, an excellent correlation is obtained by comparing the SEF (16)–with many experiments from the literature. Particularly, our model fits perfectly the experimental data if tensile and shear loadings are applied parallel or transverse to the fiber direction [3, 4], and if the shear loading angle takes 9 different values between 0 and $\frac{\pi}{2}$ [5].

It can be observed that the 10 material parameters involved in Eqs. (16) and (17) play a different role with respect to the invariants K_i: a linear dependence for b_3, b_6 and b_{24}; a quadratic dependence for a_1, a_2, a_3 and a_4; a coupling dependence (between K_2 and K_4) for a_{24}, and finally an exponential dependence for α and β. It is also noted that the proposed SEF does not contain any linear contribution with respect to K_1. This lack is due to the need of ensuring the continuity of the case-sensitive expression (17), when the stress tensor is derived from the SEF. It is also observed that a quadratic term with respect to the shear invariant K_6 is missing. This is because adding a quadratic contribution with respect to K_6 will have no effect on uniaxial tension stress (Eqs. (33) and (34)), neither on shear stress if a

shear loading is applied parallel to the fiber direction (Eq. (51)). The only effect appears if a shear loading is applied transverse to the fiber direction (Eq. (52)) and, in that case, we have checked that a quadratic contribution will not improve significantly the accuracy of the numerical results. Moreover, it is noticed that Eqs. (16)-(17) are consistent with a standard property stating that a SEF must be equal to zero if the material is at rest. Actually, if the material is at rest, the displacement is equal to zero and, from Eqs. (2)-(3), both tensors ***F*** and ***C*** are equal to the identity matrix ***I***. Consequently, it follows from Eqs. (10)-(11) that:

$$\rho_1 = \rho_2 = \rho_3 = 1 \ ; \ \ \rho_4 = \rho_5 = \rho_6 = 0 \tag{18}$$

$$K_1 = 1 \ ; \ \ K_2 = 2 \ ; \ \ K_3 = K_6 = 0 \ ; \ \ K_4 = -1 \tag{19}$$

Reporting Eq. (19) in Eqs. (16)-(17) proves that *W*=0.

Finally, in view of determining the stress from the SEF introduced by Eq. (16)-(17), it is necessary to first calculate the derivatives of *W* with respect to K_i, as defined by Eq. (13):

$$\omega_1 = \frac{\partial W}{\partial K_1} =$$

$$\begin{cases} \{a_1 + \alpha\beta K_3 exp[\beta(K_1-1)^2]\}(K_1-1) & \text{if } K_1 \geq 1 \\ 0 & \text{otherwis} \end{cases}$$

(20)

$$\omega_2 = \frac{\partial W}{\partial K_2} = a_2(K_2-2) + b_{24} + a_{24}(K_4+1) \tag{21}$$

$$\omega_3 = \frac{\partial W}{\partial K_3} = a_3 K_3 + \ \ b_3 +$$

$$\begin{cases} \frac{\alpha}{2}(exp[\beta(K_1-1)^2]-1) & \text{if } K_1 \geq 1 \\ 0 & \text{otherwise} \end{cases} \tag{22}$$

$$\omega_4 = \frac{\partial W}{\partial K_4} = a_4(K_4+1) + b_{24} + a_{24}(K_2-2) \tag{23}$$

$$\omega_6 = \frac{\partial W}{\partial K_6} = b_6 \tag{24}$$

From this calculation, it is possible to check that a material at rest is stress-less, a fact that makes sense. Because the extra pressure term *p* equals zero for a material at rest, it follows from Eq. (6) that the Cauchy stress reduces to:

$$\boldsymbol{\sigma} = 2\frac{\partial W}{\partial \boldsymbol{C}} = 2\left\{\omega_1\frac{\partial K_1}{\partial \boldsymbol{C}} + \omega_2\frac{\partial K_2}{\partial \boldsymbol{C}} + \omega_3\frac{\partial K_3}{\partial \boldsymbol{C}} + \omega_4\frac{\partial K_4}{\partial \boldsymbol{C}} + \omega_6\frac{\partial K_6}{\partial \boldsymbol{C}}\right\} \tag{25}$$

It next comes straightforwardly from Eqs. (14) and (18) that:

$$\frac{\partial K_1}{\partial \boldsymbol{C}} = \boldsymbol{M}_a \ \ ; \ \ \frac{\partial K_2}{\partial \boldsymbol{C}} = -\frac{\partial K_4}{\partial \boldsymbol{C}} = \boldsymbol{I} - \boldsymbol{M}_a \ \ ; \ \ \frac{\partial K_3}{\partial \boldsymbol{C}} = \frac{\partial K_6}{\partial \boldsymbol{C}} = \boldsymbol{0} \tag{26}$$

Reporting Eq. (26) in Eq. (25) gives:

$$\boldsymbol{\sigma} = 2\{\omega_1 \boldsymbol{M}_a + (\omega_2 - \omega_4)(\boldsymbol{I} - \boldsymbol{M}_a)\} \tag{27}$$

The coefficients ω_1, ω_2 and ω_4 are calculated by reporting Eq. (19) in Eqs. (20), (21) and (23):

$$\omega_1 = 0 \;\; ; \;\; \omega_2 = \omega_4 = b_{24} \tag{28}$$

As expected, reporting Eq. (28) in Eq. (27) finally yields to $\boldsymbol{\sigma} = \boldsymbol{0}$.

4. Closed form solutions for uniaxial tension and simple shear tests

4.1 Uniaxial tension test

Consider a cubic block of material subjected to a simple tension loading ***t*** as shown in Figure 3. The loading is applied parallel to the fiber direction (left part of Fig. 3) or transverse to the fiber direction (right part of Fig. 3). The left face (opposite to ***t***), and the two lateral faces (down and back) of the block are simply supported. The two last faces (up and front) are free.

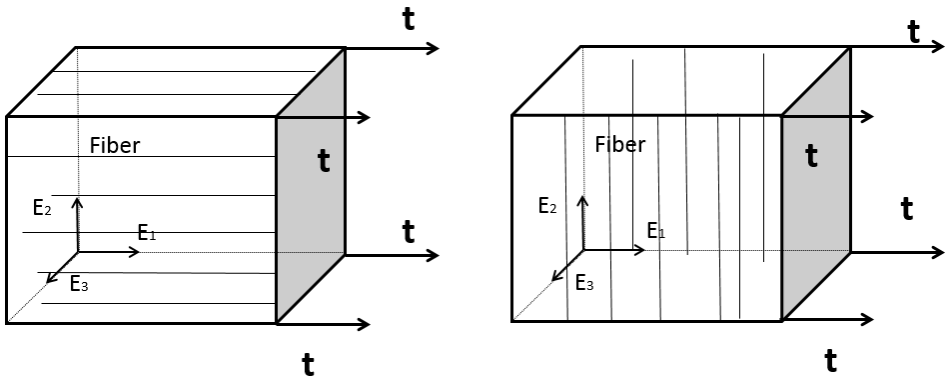

Figure 3 – *Uniaxial tension test*

By using the incompressibility condition $J = \det(\boldsymbol{F}) = \lambda_1\lambda_2\lambda_3 = 1$ (where λ_1, λ_2 and λ_3 represent the principal stretches), and by considering the loading and the boundary conditions applied to the block of material, one obtains a diagonal matrix for the deformation tensors ***F*** and ***C*** and for the stress tensor ***P***:

$$\boldsymbol{F} = \begin{pmatrix} \lambda_1 & 0 & 0 \\ 0 & \lambda_2 & 0 \\ 0 & 0 & \lambda_1^{-1}\lambda_2^{-1} \end{pmatrix} \Rightarrow \boldsymbol{C} = \begin{pmatrix} \lambda_1^2 & 0 & 0 \\ 0 & \lambda_2^2 & 0 \\ 0 & 0 & \lambda_1^{-2}\lambda_2^{-2} \end{pmatrix} \tag{29}$$

$$\boldsymbol{P} = \begin{pmatrix} P_{11}^i & 0 & 0 \\ 0 & P_{22}^i & 0 \\ 0 & 0 & P_{33}^i \end{pmatrix} \tag{30}$$

The diagonal component P_{11}^i represents the tensile stress in the loading direction, while the two other diagonal terms P_{22}^i and P_{33}^i are related to the free faces of the cubic block. The superscript *i* stands for *p* or *t*, depending on whether the loading is parallel or transverse to the fiber direction. The three diagonal components of ***P***, corresponding to these two loading cases, are given by [2]:

$$\begin{cases} P_{11}^p = 2\omega_1\lambda_1 - p\lambda_1^{-1} \;\; ; \;\; P_{22}^p = 2(\omega_2\lambda_2 - \omega_4\lambda_1^{-2}\lambda_2^{-1}) - p\lambda_2^{-1} \\ P_{33}^p = 2(\omega_2 - \omega_4\lambda_2^2)\lambda_1^{-1}\lambda_2^{-1} - p\lambda_1\lambda_2 \end{cases} \tag{31}$$

$$\begin{cases} P_{11}^t = 2(\omega_2\lambda_1 - \omega_4\lambda_1^{-1}\lambda_2^{-2}) - p\lambda_1^{-1} \;\; ; \;\; P_{22}^t = 2\omega_1\lambda_2 - p\lambda_2^{-1} \\ P_{33}^t = 2(\omega_2 - \omega_4\lambda_1^2)\lambda_1^{-1}\lambda_2^{-1} - p\lambda_1\lambda_2 \end{cases} \tag{32}$$

The free loading condition P_{33}=0 is used with the third equations of (31)-(32) for eliminating the extra pressure *p* from the two first equations of (31) and (32):

$$P_{11}^p = 2[\omega_1\lambda_1 - \omega_2\lambda_1^{-3}\lambda_2^{-2} + \omega_4\lambda_1^{-3}] \;\; ; \;\; P_{22}^p = 2\omega_2[\lambda_2 - \lambda_1^{-2}\lambda_2^{-3}] \tag{33}$$

$$P_{11}^t = 2\omega_2(\lambda_1 - \lambda_1^{-3}\lambda_2^{-2}) \;\; ; \;\; P_{22}^t = 2[\omega_1\lambda_2 - \omega_2\lambda_1^{-2}\lambda_2^{-3} + \omega_4\lambda_2^{-3}] \tag{34}$$

If the stretches λ_1 and λ_2 are switched together, it is noticed that P_{11}^p corresponds to P_{22}^t, and P_{22}^p to P_{11}^t. That makes sense because the role played by the two directions $\boldsymbol{E}_1$ and $\boldsymbol{E}_2$ is reversed if the loading is applied parallel or transverse to the fiber direction.

In order to calculate the three coefficients ω_1, ω_2 and ω_4 involved in Eqs. (33)-(34), the three vectors ***a***, ***b*** and ***c*** are determined from Eqs. (8)-(9):

$$\theta = 0: \qquad \boldsymbol{a} = \begin{pmatrix} 1 \\ 0 \\ 0 \end{pmatrix} \;\; ; \;\; \boldsymbol{b} = \begin{pmatrix} 0 \\ 1 \\ 0 \end{pmatrix} \;\; ; \;\; \boldsymbol{c} = \begin{pmatrix} 0 \\ 0 \\ 1 \end{pmatrix} \tag{35}$$

$$\theta = \frac{\pi}{2}: \qquad \boldsymbol{a} = \begin{pmatrix} 0 \\ 1 \\ 0 \end{pmatrix} \;\; ; \;\; \boldsymbol{b} = \begin{pmatrix} -1 \\ 0 \\ 0 \end{pmatrix} \;\; ; \;\; \boldsymbol{c} = \begin{pmatrix} 0 \\ 0 \\ 1 \end{pmatrix} \tag{36}$$

Eqs. (10), (11), (35) and (36) next yield to:

$$\theta = 0: \;\; \begin{cases} \rho_1 = \lambda_1^2 \;\; ; \;\; \rho_2 = \lambda_2^2 \;\; ; \;\; \rho_3 = \lambda_1^{-2}\lambda_2^{-2} \;\; ; \;\; \rho_4 = \rho_5 = \rho_6 = 0 \\ K_1 = \lambda_1^2 \;\; ; \;\; K_2 = \lambda_2^2 + \lambda_1^{-2}\lambda_2^{-2} \;\; ; \;\; K_3 = K_6 = 0 \;\; ; \;\; K_4 = -\lambda_1^{-2} \end{cases} \tag{37}$$

$$\theta = \frac{\pi}{2}: \;\; \begin{cases} \rho_1 = \lambda_2^2 \;\; ; \;\; \rho_2 = \lambda_1^2 \;\; ; \;\; \rho_3 = \lambda_1^{-2}\lambda_2^{-2} \;\; ; \;\; \rho_4 = \rho_5 = \rho_6 = 0 \\ K_1 = \lambda_2^2 \;\; ; \;\; K_2 = \lambda_1^2 + \lambda_1^{-2}\lambda_2^{-2} \;\; ; \;\; K_3 = K_6 = 0 \;\; ; \;\; K_4 = -\lambda_2^{-2} \end{cases} \tag{38}$$

ω_1, ω_2 and ω_4 can then be calculated from Eqs. (20), (21), (23), (37) and (38):

$$\theta = 0: \quad \begin{cases} \omega_1 = a_1(\lambda_1^2 - 1) \ ; \ \ \omega_2 = a_2(\lambda_2^2 + \lambda_1^{-2}\lambda_2^{-2} - 2) + b_{24} + a_{24}(1 - \ \lambda_1^{-2}) \\ \omega_4 = a_4(1 - \ \lambda_1^{-2}) + b_{24} + a_{24}(\lambda_2^2 + \lambda_1^{-2}\lambda_2^{-2} - 2) \end{cases} \tag{39}$$

$$\theta = \frac{\pi}{2}: \quad \begin{cases} \omega_1 = 0 \ ; \ \ \omega_2 = a_2(\lambda_1^2 + \lambda_1^{-2}\lambda_2^{-2} - 2) + b_{24} + a_{24}(1 - \ \lambda_2^{-2}) \\ \omega_4 = a_4(1 - \ \lambda_2^{-2}) + b_{24} + a_{24}(\lambda_1^2 + \lambda_1^{-2}\lambda_2^{-2} - 2) \end{cases} \tag{40}$$

As a consequence of the case-sensitive expression (20), ω_1 is equal to zero if $\theta = \frac{\pi}{2}$ while it is not if $\theta = 0$. Actually, in the case of a tensile loading parallel to the fiber direction ($\theta = 0$), it results from Eq. (37) that $K_1 = \lambda_1^2 \geq 1$, giving a non-zero contribution for ω_1. On the contrary, in the case of a tensile loading transverse to the fiber direction $\left(\theta = \frac{\pi}{2}\right)$, it results from Eq. (38) that $K_1 = \lambda_2^2 \leq 1$ since the lateral free faces of the block of material are shrunk. In this situation, as a consequence of the case-sensitive expression (20), ω_1 is equal to zero. In order to express the tensile stress with respect to the stretches λ_1 and λ_2, we finally report Eqs. (39)-(40) in Eqs. (33)-(34):

$$\begin{aligned} P_{11}^p = 2[&(\lambda_1^2 - 1)\lambda_1 a_1 - (\lambda_2^2 + \lambda_1^{-2}\lambda_2^{-2} - 2)\lambda_1^{-3}\lambda_2^{-2}a_2 + (1 - \lambda_1^{-2})\lambda_1^{-3}a_4 \\ &+(\lambda_2^2 + 2\lambda_1^{-2}\lambda_2^{-2} - 2 - \lambda_2^{-2})\lambda_1^{-3}a_{24} + (1 - \lambda_2^{-2})\lambda_1^{-3}b_{24}] \end{aligned} \tag{41}$$

$$P_{22}^p = 2[a_2(\lambda_2^2 + \lambda_1^{-2}\lambda_2^{-2} - 2) + b_{24} + a_{24}(1 - \ \lambda_1^{-2})][\lambda_2 - \lambda_1^{-2}\lambda_2^{-3}] \tag{42}$$

$$P_{11}^t = 2[a_2(\lambda_1^2 + \lambda_1^{-2}\lambda_2^{-2} - 2) + b_{24} + a_{24}(1 - \ \lambda_2^{-2})][\lambda_1 - \lambda_1^{-3}\lambda_2^{-2}] \tag{43}$$

$$\begin{aligned} P_{22}^t = 2[&-(\lambda_1^2 + \lambda_1^{-2}\lambda_2^{-2} - 2)\lambda_1^{-2}\lambda_2^{-3}a_2 + (1 - \lambda_2^{-2})\lambda_2^{-3}a_4 \\ &+(\lambda_1^2 + 2\lambda_1^{-2}\lambda_2^{-2} - 2 - \lambda_1^{-2})\lambda_2^{-3}a_{24} + (1 - \lambda_1^{-2})\lambda_2^{-3}b_{24}] \end{aligned} \tag{44}$$

It is observed that the stresses described by Eqs. (41)-(44) depend on 5 material parameters (a_1, a_2, a_4, b_{24} and a_{24}), among the 10 embedded in the model, and also on the two stretches λ_1 and λ_2. During a uniaxial tensile stress, λ_1 is always a known data while λ_2 can be measured [3] or not [4]. If λ_2 has been measured, the measurements are reported in Eqs. (41) and (43) for calculating the tensile stress. It is then noted that the dependence of the tensile stresses is linear with respect to the material parameters. On the contrary, if λ_2 is not measured during the experiments, we have to calculate it from Eqs. (42) and (44) by using the free loading condition $P_{22} = 0$:

$$\theta = 0: \qquad \lambda_2 = \frac{1}{\sqrt{\lambda_1}} \tag{45}$$

$$\theta = \frac{\pi}{2}: \qquad \lambda_2^2 = \frac{a_2 - 2a_{24}\lambda_1^2 + a_4\lambda_1^4}{\lambda_1^2(2a_2 - b_{24} - a_{24} + (a_4 - a_2 + b_{24} - 2a_{24})\lambda_1^2 + a_{24}\lambda_1^4)} \tag{46}$$

It can be noted that Eq. (45) can also be found by using the incompressibility condition

$\lambda_1\lambda_2\lambda_3 = 1$. The two directions $\boldsymbol{E}_2$ and $\boldsymbol{E}_3$ actually play the same role if $\theta = 0$, and thus λ_2=λ_3. Using this equality with $\lambda_1\lambda_2\lambda_3 = 1$ gives $\lambda_1\lambda_2^2 = 1$, which is equivalent to (45). Also note that reporting Eq. (45) in Eq. (41) does not change the nature of the tensile stress with respect to the material parameters which is still linear. However, if $\theta = \frac{\pi}{2}$, reporting Eq. (46) in Eq. (43) leads to a situation where the tensile stress depends nonlinearly on the 4 material parameters a_2, a_4, b_{24} and a_{24}. All these observations are of prime importance in order to select the appropriate optimization process for identifying the material parameters of the model. This identification will be performed in Section 5.

4.2 Simple shear test

A shear experiment is driven by the shear deformation k which is considered as a known data. As shown in Figure 4, the field displacement $\boldsymbol{U}$ related to a block of material subjected to a simple shear deformation is expressed in a linear form with respect to k:

$$\boldsymbol{U} = kX_2\boldsymbol{E}_1 \tag{47}$$

It follows from Eqs. (2)-(3) that the corresponding strain tensors are:

$$\boldsymbol{F} = \begin{pmatrix} 1 & k & 0 \\ 0 & 1 & 0 \\ 0 & 0 & 1 \end{pmatrix} \Rightarrow \boldsymbol{C} = \begin{pmatrix} 1 & k & 0 \\ k & k^2+1 & 0 \\ 0 & 0 & 1 \end{pmatrix} \tag{48}$$

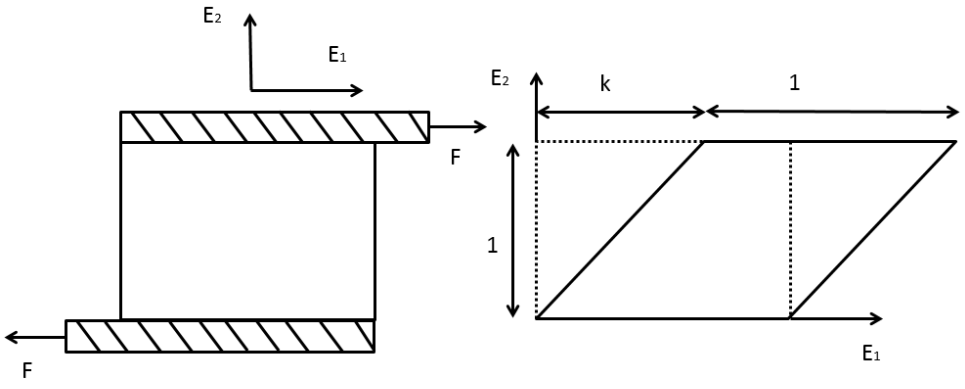

Figure 4 – *Simple shear test*

Prior to calculate the stress tensor, we first need to determine the invariants K_i and their related coefficients ρ_i from Eqs. (10)-(11):

$$\begin{cases} \rho_1 = 1 + k^2 s^2 + 2kcs \;\; ; \;\; \rho_2 = 1 + k^2 c^2 - 2kcs \;\; ; \;\; \rho_3 = 1 \\ \rho_4 = k(c^2 - s^2) + k^2 sc \;\; ; \;\; \rho_5 = \rho_6 = 0 \end{cases} \quad (49)$$

$$\begin{cases} K_1 = 1 + k^2 s^2 + 2kcs \;\; ; \;\; K_2 = 2 + k^2 c^2 - 2kcs \;\; ; \;\; K_3 = k^2 (c^2 - s^2 + kcs)^2 \\ K_4 = -1 - k^2 c^2 + 2kcs \;\; ; \;\; K_6 = k^3 (c^2 - s^2 + kcs)^2 (kc^2 - 2cs) \end{cases} \quad (50)$$

Since the angle θ belongs to the interval $\left[0, \frac{\pi}{2}\right]$, c and s are positive, and then K_1 is larger than 1. The first occurrence of the case-sensitive expressions (20) and (22) must therefore be used. In the particular case of a loading parallel $(c = 1, s = 0)$ or transverse $(c = 0, s = 1)$ to the fiber direction, the nominal shear stress component adopts a simple form as reported in [2]:

$$\theta = 0: \quad P_{12} = 2[(\omega_2 + \omega_3 - \omega_4)k - \omega_4 k^3] \quad (51)$$

$$\theta = \frac{\pi}{2}: \; P_{12} = 2[(\omega_2 + \omega_3 - \omega_4)k - \omega_6 k^3] \quad (52)$$

In order to calculate the coefficients ω_2, ω_3, ω_4 and ω_6 of Eqs. (51)-(52) with respect to the fiber angle θ, we report Eq. (50) in Eqs. (21)-(24):

$$\theta = 0: \quad \begin{cases} \omega_2 = (a_2 - a_{24})k^2 + b_{24} \;\; ; \;\; \omega_3 = a_3 k^2 + \;\; b_3 \\ \omega_4 = (a_{24} - a_4)k^2 + b_{24} \;\; ; \;\; \omega_6 = b_6 \end{cases} \quad (53)$$

$$\theta = \frac{\pi}{2}: \omega_2 = b_{24} \;\; ; \;\; \omega_3 = a_3 k^2 + \;\; b_3 + \frac{\alpha}{2}(exp[\beta k^4] - 1) \;\; ; \;\; \omega_4 = b_{24} \;\; ; \;\; \omega_6 = b_6 \quad (54)$$

And, by reporting Eqs. (53)-(54) in Eqs. (51)-(52):

$$\theta = 0: \; P_{12} = 2[b_3 k + (a_2 + a_4 - 2a_{24} + a_3 - b_{24})k^3 + (a_4 - a_{24})k^5] \quad (55)$$

$$\theta = \frac{\pi}{2}: \quad P_{12} = 2\left[\left(b_3 - \frac{\alpha}{2}\right)k + (a_3 - b_6)k^3 + \frac{\alpha}{2} exp[\beta k^4]k\right] \quad (56)$$

In Eqs. (55) and (56), it is noticed a difference of $-\alpha k$ between the linear terms with k, meaning that the linear contributions have a different slope. The initial linear slope is actually equal to $2b_3$ for a shear loading parallel to the fiber direction while this initial linear slope is equal to $2b_3 - \alpha$ for a shear loading transverse to the fiber direction. Hence, the two initial linear slopes are not equal with a difference driven by the material parameter α and condition 2 introduced in section 3 is fulfilled. This particularity is of a major importance in view of fitting properly the experimental shear stress extracted from [3]. Actually, this shear stress behaves linearly with k (Fig. 2), but with a different slope depending on if the shear loading is applied parallel or transverse to the fiber direction. Our model is therefore able to well predict this kind of behavior (Fig. 8 and 10).

However, as reported in [5], it is also possible to be faced to a shear loading not necessarily

parallel or transverse to the fiber direction. In such situations, we have to establish more general formulas than Eqs. (55)-(56) by first reporting Eqs. (8)-(9) in (15), and next reporting the result in Eq. (14):

$$\begin{cases} \dfrac{\partial K_1}{\partial c} = \begin{pmatrix} c^2 & cs & 0 \\ cs & s^2 & 0 \\ 0 & 0 & 0 \end{pmatrix}; \ \dfrac{\partial K_2}{\partial c} = \begin{pmatrix} s^2 & -cs & 0 \\ -cs & c^2 & 0 \\ 0 & 0 & 1 \end{pmatrix}; \\ \dfrac{\partial K_3}{\partial c} = k(c^2 - s^2 + kcs) \begin{pmatrix} -2cs & c^2 - s^2 & 0 \\ c^2 - s^2 & 2cs & 0 \\ 0 & 0 & 0 \end{pmatrix} \\ \dfrac{\partial K_4}{\partial c} = \begin{pmatrix} -s^2 & sc & 0 \\ sc & -c^2 & 0 \\ 0 & 0 & -1 - k^2c^2 + 2kcs \end{pmatrix} \\ \dfrac{\partial K_6}{\partial c} = k^2(c^2 - s^2 + kcs)c(kc - 2s) \begin{pmatrix} -2cs & c^2 - s^2 & 0 \\ c^2 - s^2 & 2cs & 0 \\ 0 & 0 & 0 \end{pmatrix} \\ + k^2(c^2 - s^2 + kcs)^2 \begin{pmatrix} s^2 & -cs & 0 \\ -cs & c^2 & 0 \\ 0 & 0 & -1 \end{pmatrix} \end{cases} \tag{57}$$

It follows straightforwardly from Eqs. (6), (20)-(24), (48), (50) and (57) that the Cauchy stress tensor adopts the particular form:

$$\boldsymbol{\sigma} = \begin{pmatrix} \sigma_{11} & \sigma_{12} & 0 \\ \sigma_{12} & \sigma_{22} & 0 \\ 0 & 0 & \sigma_{33} \end{pmatrix} \tag{58}$$

$$\begin{aligned} \sigma_{12} = 2\{ & ks^2(ks + c)(ks + 2c)a_1 + kc^2(kc - s)(kc - 2s)(a_2 + a_4 - 2a_{24}) \\ & + k^3(c^2 - s^2 + kcs)^3(c^2 - s^2 + 2kcs)a_3 + k(c^2 - s^2 + kcs)(c^2 - s^2 + 2kcs)b_3 \\ & + k^2c(c^2 - s^2 + kcs)[(kc - 2s)(c^2 - s^2 + 2kcs) + (kc - s)(c^2 - s^2 + kcs)]b_6 \\ & + k(c^2 - s^2 + kcs)[exp(\beta[ks(ks + 2c)]^2)\beta(ks)^2(ks + c)(ks + 2c) \\ & + \tfrac{c^2 - s^2 + 2kcs}{2}(exp(\beta[ks(ks + 2c)]^2) - 1)\Big]\alpha\Big\} \end{aligned} \tag{59}$$

$$\begin{aligned} \sigma_{22} = 2\{ & ks^3(ks + 2c)a_1 - kcs^2(kc - 2s)(a_2 - a_{24}) + 2k^3cs(c^2 - s^2 + kcs)^3a_3 \\ & + (kc - s)^2kc(2s - kc)(a_4 - a_{24}) + kc(kc - 2s)b_{24} + 2kcs(c^2 - s^2 + kcs)b_3 \\ & + k^2(c^2 - s^2 + kcs)[(c^2 - s^2 + kcs)(1 + c^2) + 2c^2s(kc - 2s)]b_6 \\ & + ks(c^2 - s^2 + kcs)[exp(\beta[ks(ks + 2c)]^2)\beta(ks)^2(ks + 2c)(c^2 - s^2 + kcs) \\ & + c(exp(\beta[ks(ks + 2c)]^2) - 1)]\alpha\} \end{aligned} \tag{60}$$

Note that the extra pressure p was eliminated from Eqs. (59)-(60) by using the plane stress condition $\sigma_{33} = 0$. It is also noted that all the 10 material parameters of the model are involved in the stress expressions, except b_{24} which is only concerned by the normal stress

σ_{22}. It is finally observed that the material parameters a_{24} appears in Eq. (60) with the expressions $a_2 - a_{24}$ and $a_4 - a_{24}$ while it appears in Eq. (59) with the expression $a_2 + a_4 - 2a_{24}$. We can therefore deduce from the basic equality $a_2 + a_4 - 2a_{24} = (a_2 - a_{24}) + (a_4 - a_{24})$ that a_{24}, a_2 and a_4 are not independent material parameters. This is why only $a_2 - a_{24}$ and $a_4 - a_{24}$ are provided in Table 6. Performing an identification process based on only shear experiments using the stress components σ_{12} and σ_{22} only allows to identify 9 of the 10 material parameters of our model.

5. Material parameter identification

In order to identify the 10 material parameters a_1, a_2, a_3, a_4, a_{24}, b_3, b_6, b_{24}, α and β of our model, we have used the classical coefficient of determination R^2:

$$R^2 = 1 - \frac{S_{res}}{S_{tot}} \tag{61}$$

Where S_{res} and S_{tot} are respectively the residual sum and the total sum of squares over the number of experimental data *n*:

$$S_{res} = \|\boldsymbol{y} - \boldsymbol{f}\|^2 = \sum_{i=1}^{n}(y_i - f_i)^2 \;\; ; \;\; S_{tot} = \|\boldsymbol{y} - \bar{\boldsymbol{y}}\|^2 = \sum_{i=1}^{n}(y_i - \bar{y})^2 \tag{62}$$

y_i stands for the experimental data, f_i for the theoretical data and $\bar{y}$ for the mean of the experimental data:

$$\bar{y} = \frac{1}{n}\sum_{i=1}^{n} y_i \tag{63}$$

The closest to 1 R^2 is, the best the fit of the experimental data by the theoretical data will be. The aim is thus to find the set of material parameters $(a_1, a_2, a_3, a_4, a_{24}, b_3, b_6, b_{24}, \alpha, \beta)$ minimizing the ratio $\frac{S_{res}}{S_{tot}}$.

5.1 Optimization strategies

As outlined before, the nature of the theoretical stress is partly linear and partly nonlinear with the material parameters, depending on the loading condition. For example, if the stretch λ_2 is known, Eqs. (41)-(43) show that the two tensile stresses, parallel and transverse to the fiber direction, are linear with respect to a_1, a_2, a_4, a_{24} and b_{24}. On the contrary, if the stretch λ_2 is unknown, it is necessary to report Eqs. (45)-(46) in Eqs. (41)-(43) and the tensile stress transverse to the fiber direction becomes nonlinear with respect to a_2,

a_4, a_{24} and b_{24} while the tensile stress parallel to the fiber direction remains linear. Regarding the shear stress, if the loading is parallel to the fiber direction, Eq. (55) shows a linear dependence with respect to a_2, a_4, a_{24} and b_3 while Eq. (56) shows a linear dependence with respect to a_3, b_3, b_6 and α but a nonlinear dependence with respect to β. In the general case of any shear angle, Eqs. (59)-(60) show that the dependence is linear with respect to 9 of 10 material parameters, namely a_1, a_2, a_3, a_4, a_{24}, b_3, b_6, a_{24}, b_{24} and α, while the dependence is nonlinear with respect to β. All these remarks suggest that it could be possible to take advantage of all the existing linear dependences in order to elaborate efficient optimization algorithms. The strategy consisting in splitting the material parameters in two categories, linear and nonlinear, has been already used in [19]. In this context, we note ***lp*** the vector storing the linear material parameters, and ***nlp*** the vector storing the nonlinear ones. With these notations the theoretical stress ***f*** can be written in a generic form as follows:

$$\boldsymbol{f} = \sum_{j=1}^{N_{lp}} lp_j \, \boldsymbol{v}_j \tag{64}$$

Where N_{lp} stands for the number of linear material parameters included in the model. The N_{lp} vectors $\boldsymbol{v}_j$ are built according to the theoretical equations (41), (43), (45), (46), (55), (56), (59) and (60). Each of them:

- is of dimension n,
- stores the stress contribution corresponding to each of the n stretches λ_1 (or of the n shear deformation k) measured during the experiments,
- is associated with the linear material parameter lp_j,
- depends on the nonlinear material parameters stored in ***nlp***.

In order to minimize the objective function $\frac{S_{res}}{S_{tot}}$, Eq. (64) is reported in the left equation of (62):

$$S_{res} = \|\boldsymbol{y}\|^2 + \|\boldsymbol{f}\|^2 - 2\langle \boldsymbol{y}, \boldsymbol{f} \rangle = \|\boldsymbol{y}\|^2 + \langle \boldsymbol{lp}, \boldsymbol{M} \ \ \boldsymbol{lp} \rangle - 2\langle \boldsymbol{b}, \boldsymbol{lp} \rangle \tag{65}$$

M is a N_l x N_l matrix whose components are defined by $M_{jk} = \langle \boldsymbol{v}_j, \boldsymbol{v}_k \rangle$ and ***b*** is a N_l-dimension vector of component: $b_j = \langle \boldsymbol{y}, \boldsymbol{v}_j \rangle$. Because the vectors $\boldsymbol{v}_j$ depend on the nonlinear material parameters ***nlp***, the matrix ***M*** and the vector ***b*** too: ***M(nlp), b(nlp)***. Note that we have considered S_{res} instead of $\frac{S_{res}}{S_{tot}}$ because S_{tot} does not depend on the material parameters. Minimizing S_{res} with respect to the material parameters is therefore

equivalent to the minimization of $\frac{S_{res}}{S_{tot}}$. From a practical point of view, we have implemented $\frac{S_{res}}{S_{tot}}$ because a relative criterion is numerically better than an absolute one. However, for the sake of simplicity, we will keep S_{res} in the following for the theoretical calculation. In the RHS of Eq. (65), the first term is a constant value with respect to the linear material parameters ***lp***, the dependence of the second term is quadratic with ***lp*** and linear with the third. We are thus faced to a standard least square optimization problem and the solution is easily found by deriving the RHS of Eq. (65) with respect to $\boldsymbol{lp}$:

$$\boldsymbol{M}(\boldsymbol{nlp})\ \ \boldsymbol{lp} = \boldsymbol{b}(\boldsymbol{nlp}) \tag{66}$$

Note that Eq. (66) is a linear system with respect to ***lp***, but not with respect to ***nlp***. We therefore need to solve iteratively Eq. (66) inside a loop. We have implemented this loop in the Octave free software [16], and the optimization related to the nonlinear material parameters was performed with the *fminbnd* or *fminsearch* functions, depending on if the number of nonlinear parameters is one or strictly greater that one. The corresponding algorithm is presented in Figure 5. It should be noted that splitting the material parameters into two categories allows to save computation time because the optimization related to the nonlinear material parameters concerns a small number of parameters and solving the linear system (66) with respect to the linear material parameters is very fast.

- Step 1: Set a tolerance value ε
- Step 2: Set the initial values of the linear and nonlinear parameters ***lp*** and ***nlp***
- Step 3: Calculate the objective function S_{res} with Eq. (65)
- Step 4: Optimization loop

  Do while $S_{res} > \varepsilon$

  Update ***nlp*** by minimizing S_{res} (*fminbnd* or *fminsearch)*

  Update ***lp*** by solving the linear system (66)

  Update the objective function S_{res} with Eq. (65)

  Enddo

Figure 5 – *Flow chart of the optimization process in the case where λ_2 is an unknown data*

However, in some circumstances of tensile loading, the free boundary condition $P_{22} = 0$

must be included in the optimization process. For example, if λ_2 is known from experimental measurements, we do not need to use Eqs. (42) and (44) to get λ_2. In such a case, the free boundary condition $P_{22} = 0$ is not automatically satisfied while it must hold. On the contrary, if the stretch λ_2 is unknown, we use Eqs. (42) and (44) to get λ_2 and the condition $P_{22} = 0$ is automatically satisfied. Several strategies to enforce a stress to be zero during an optimization process are discussed in [20]. One of the main difficulties comes from the necessity to work with a relative objective function because we have to divide S_{res} by S_{tot}, and S_{tot} is equal to zero if P_{22} is equal to zero. To overcome this difficulty, we propose an original method based on a spectral analysis. This method consists in using again Eq. (66), but with a null vector instead of ***b*** since ***y*** is now equal to zero:

$$\boldsymbol{M}^{22}(\boldsymbol{nlp})\ \ \boldsymbol{lp} = \boldsymbol{0} \tag{67}$$

The superscript ^{22} is introduced in Eq. (67) in order to refer to the stress component P_{22}, and also to avoid any misunderstanding with the matrix ***M***(***nlp***) of Eq. (66). A non-trivial solution of Eq. (67), that is to say a non-zero vector ***lp***, is provided by the eigenvectors of $\boldsymbol{M}^{22}(\boldsymbol{nlp})$ related to a null eigenvalue. It is therefore possible to expand ***lp*** with an eigenvector basis, says ***eig***, related to the 0 proper vector subspace (of dimension N_0) of $\boldsymbol{M}^{22}(\boldsymbol{nlp})$:

$$\boldsymbol{lp} = \sum_{p=1}^{N_0} a_p\, \boldsymbol{eig}_p \tag{68}$$

Eq. (68) is next reported in Eq. (65):

$$S_{res} = \|\boldsymbol{y}\|^2 + \langle \boldsymbol{a}, \boldsymbol{N}\ \ \boldsymbol{a}\rangle - 2\langle \boldsymbol{c}, \boldsymbol{a}\rangle \tag{69}$$

N is a N_0 x N_0 matrix whose components are defined by $N_{pq} = \langle \boldsymbol{eig}_p, \boldsymbol{M}\ \ \boldsymbol{eig}_q\rangle$, ***c*** is a N_0-dimension vector of component $c_p = \langle \boldsymbol{b}, \boldsymbol{eig}_p\rangle$, and ***a*** is a N_0-dimension vector storing the component a_p of ***lp*** in the eigenvector's expansion (68). Because ***N*** and ***c*** are related to ***M*** and ***b***, they also depend on the nonlinear material parameters ***nlp***: ***N(nlp), c(nlp)***. Eq. (69) is again a standard least square optimization problem whose solution is easily found by deriving the RHS of Eq. (69) with respect to ***a***:

$$\boldsymbol{N}(\boldsymbol{nlp})\ \ \boldsymbol{a} = \boldsymbol{c}(\boldsymbol{nlp}) \tag{70}$$

We have therefore obtained an equation similar to Eq. (66), but with a lower size since N_0 is lower than N_I. N_0 is actually the dimension of a proper vector subspace included in a vector

space of dimension N_l. Since Eq. (70) is a linear system with respect to ***a***, but not with respect to ***nlp***, we need to solve it iteratively inside a loop. The corresponding algorithm developed with Octave is presented in Figure 6.

- Step 1: Set a tolerance value ε
- Step 2: Set the initial values of the linear and nonlinear parameters ***lp*** and ***nlp***
- Step 3: Calculate the objective function S_{res} with Eq. (65)
- Step 4: Optimization loop

  Do while $S_{res} > \varepsilon$

    Update ***nlp*** by minimizing S_{res} (*fminbnd* or *fminsearch)*

    Compute the eigenvectors of $\boldsymbol{M}^{22}(\boldsymbol{nlp})$ related to the eigenvalue 0

    Update ***a*** by solving the linear system (70)

    Update ***lp*** by using the spectral decomposition (68)

    Update the objective function S_{res} with Eq. (65)

  Enddo

Figure 6 – *Flow chart of the optimization process in the case where λ_2 is a known data*

5.2 Comparison between the model (16) and the data of Ciarletta et al. [3]

The experimental data obtained in [3] are used in this section as a reference to identify the material parameters of our model. These data concern two different fiber-reinforced rubbers materials under uniaxial tension and shear deformations, with a loading direction parallel or transverse to the fiber direction. The materials are made of soft silicone rubbers reinforced by polyamide or hard silicone rubber. These two kinds of materials are respectively referenced as Mat. A and Mat. B. The corresponding material parameters are shown in Tables 1 and 2. They were identified by using the algorithm of Figure 6 because λ_2 was measured during the tensile test in [3]. The stress prediction was computed by applying the following analytical formulas: Eqs. (41) and (43) for the tensile loading and Eqs. (55)-(56) for the shear loading.

a_1	a_2	a_3	a_4	a_{24}
0.049	0.030	0.073	0.27	0.081

b_3	b_6	b_{24}	α	β
0.043	-0.85	0.069	-0.18	-6.2 10^{10}

Table 1 – *Identified material parameters – Mat. A*

a_1	a_2	a_3	a_4	a_{24}
1.48	0.24	-2.05	4.7	1.5
b_3	b_6	b_{24}	α	β
0.093	-40	0.73	-11	-2.9 10^{10}

Table 2 – *Identified material parameters – Mat. B*

The comparisons between the experimental and the numerical results are presented on Figures 7 and 8 for Mat. A and on Figures 9 and 10 for Mat. B. From these figures, we can observe that the numerical results match very well the experimental data. This is confirmed by the coefficients of determination R^2 presented in Table 3. Compared to the best model proposed in [2], we find the same coefficient of determination for Mat. A, and almost the same for Mat. B, with a reduction of the number of material parameters from 23 to 10. In the case of material B, it is observed that two loadings (Figs. 9a and 10a) provide result slightly worse than the two others (Figs. 9b and 10b). In Fig. 9a, the behavior curve presents several curvature changes: first concave, then convex, and finally slightly concave. This kind of behavior is difficult to predict, especially in a situation where we need to match simultaneously 4 loading cases. Fig. 10a concerns a situation where the experimental data are scattered with a large standard deviation, and it is well known that fitting such experimental data is challenging. By using a model including more than 10 material parameters, such as in [2] with 23 material parameters, it is possible to improve the accuracy, with a coefficient of determination R^2 changing from 0.98 to 0.99 and from 0.97 to 0.99 respectively, as reported in Table 3. However, this is a very slight increase and the price to pay for improving results by so little does not worth it.

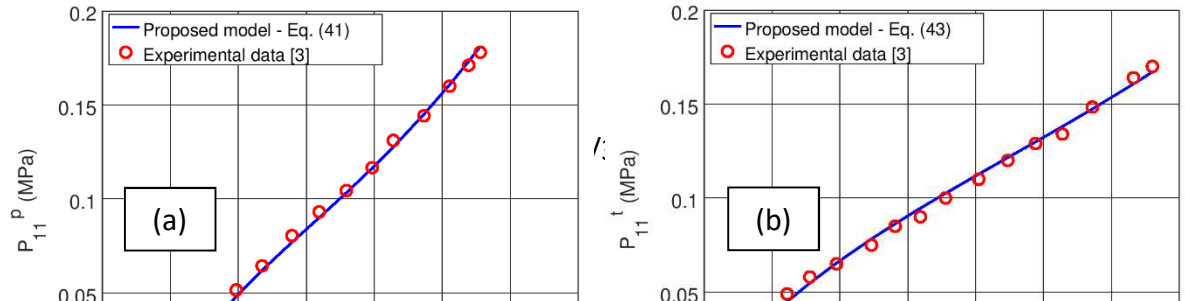

Figure 7 – *Tensile stress Mat. A – loading parallel (a) and transverse (b) to the fiber direction*

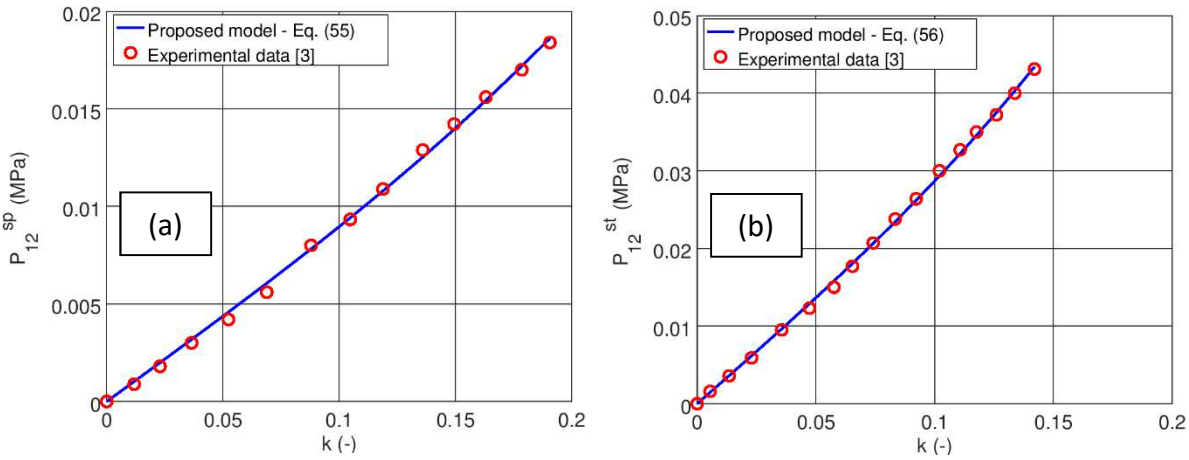

Figure 8 – *Shear stress Mat. A – loading parallel (a) and transverse (b) to the fiber direction*

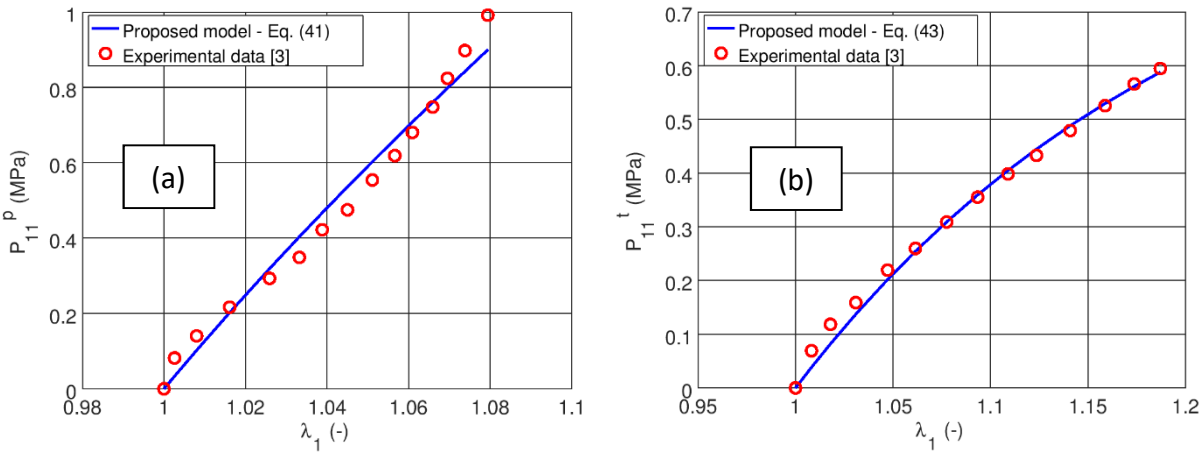

Figure 9 – *Tensile stress Mat. B – loading parallel (a) and transverse (b) to the fiber direction*

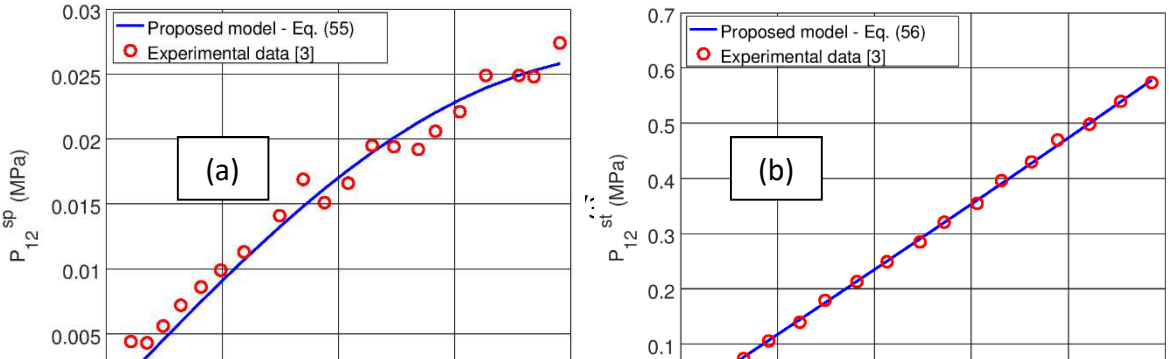

Figure 10 – *Shear stress Mat. B – loading parallel (a) and transverse (b) to the fiber direction*

SEF	Tension				Shear			
	parallel		transverse		parallel		transverse	
	Mat A	Mat B	Mat A	Mat B	Mat A	Mat B	Mat A	Mat B
Eqs. (16)-(17)	1	0.98	1	0.99	1	0.97	1	1
Eq. (75) in [2]	1	0.99	1	0.99	1	0.99	1	1

Table 3 – *Coefficient of determination* R^2

5.3 Comparison between the model (16) and the data of Davis et al. [4]

In this section, we consider uniaxial tension deformation and simple shear deformation of human medial collateral ligament (MCL) tissue. Quapp et al. [21] performed experiments on this kind of tissue under the cases of uniaxial tension deformation parallel and transverse to the fiber direction. Davis et al. [4] used later these experimental data to determine material parameters and to make predictions for simple shear parallel and transverse to the fiber direction. We compare our SEF with these two sets of experimental data covering a large scope of the material behavior. The values of material parameters for MCL tissue (Table 4) were determined by using the optimization method described in Section 5.1 and by applying the closed form solutions exhibited in Section 4. More precisely, the identification process was performed by using the algorithm of Figure 5 because λ_2 has not been measured during the experiments. Eqs. (45)-(46) were thus used to compute λ_2. The stress prediction is next calculated by applying the following analytical formulas: Eqs. (41) and (43) for the tensile loading and Eqs. (55)-(56) for the shear loading. The comparison between our model and the data extracted from [4] are shown in Figures 11 and 12. It is observed an excellent agreement confirmed by the corresponding coefficients of correlation (Table 5). The worst

case (R^2=0.99 in Fig. 11a) concerns a situation where the behavior curve presents several curvature changes: first concave, then convex, and finally slightly concave. As observed previously in section 5.2, these changes of curvature are difficult to predict, especially in a context where we need to match simultaneously four loading cases and find the best balance between them.

a_1	a_2	a_3	a_4	a_{24}
40	12136	-9.05	12808	12465
b_3	b_6	b_{24}	α	β
2.1	-65	1.1	46	11

Table 4 – *Identified material parameters – MCL*

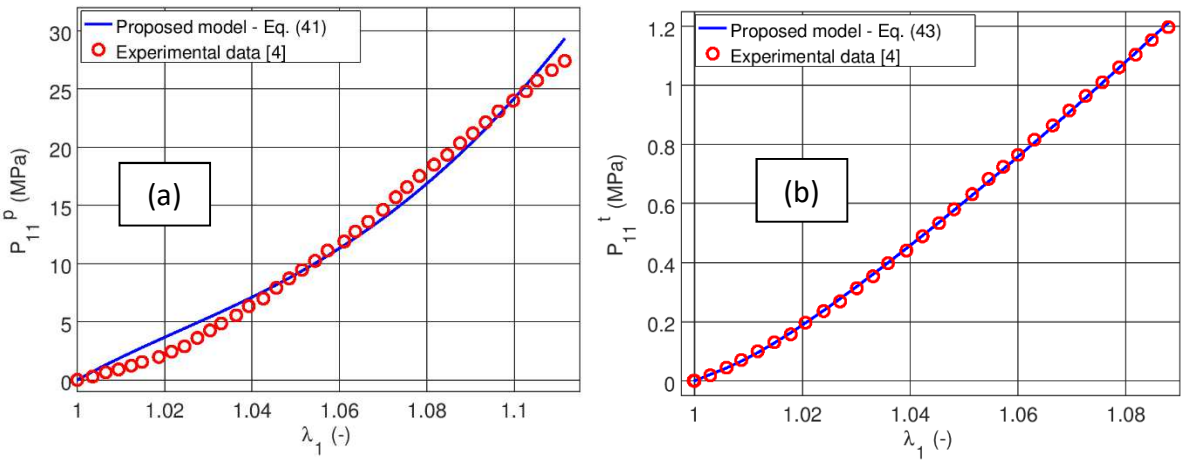

Figure 11 – *Tensile stress MCL – loading parallel (a) and transverse (b) to the fiber direction*

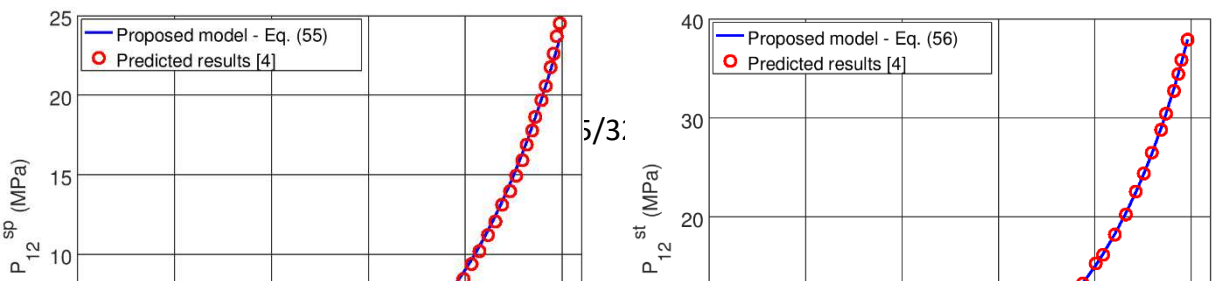

Figure 12 – *Shear stress MCL – loading parallel (a) and transverse (b) to the fiber direction*

SEF	Tension		Shear	
	parallel	transverse	parallel	transverse
Eqs. (16)-(17)	0.99	1	1	1

Table 5 – *Coefficient of determination* R^2 *for MCL*

5.4 Comparison between the model (16) and the data of Horgan et al. [5]

Horgan et al. [5] used recent experimental data, obtained by Feng et al. [22] with porcine brain white matter, to perform simple shear computations with 9 different values of the angle θ. We have used these 9 simple shear simulations as a reference for identifying 9 of the 10 material parameters of our model (Table 6). As previously highlighted with Eqs. (59)-(60), it is actually reminded that using shear tests is not sufficient for identifying all the material parameters. It should be also outlined that the stresses are normalized in this section by a shear modulus μ equal to 1.49 kPa, according to [5]. This value of μ was previously determined in [22]. The values of material parameters for porcine brain white matter were identified by using the optimization method described in section 5.1 and by applying the closed form solutions exhibited in section 4. More precisely, the identification process was performed by using the algorithm of Figure 5 because it is obvious that λ_2 is not measured during a shear test. The stress prediction is computed by applying the analytical formulas (59) for the shear stress and (60) for the normal stress. The comparisons between our model and the Horgan computations are shown in Figure 13. It is observed an excellent

agreement confirmed by the corresponding coefficients of correlation (Table 7).

a_1	$a_2 - a_{24}$	a_3	$a_4 - a_{24}$	
7.7 10^{-3}	4.05 10^{-5}	1.2 10^{-3}	-2.3 10^{-6}	
b_3	b_6	b_{24}	α	β
1.4 10^{-3}	-5.8 10^{-4}	8.1 10^{-4}	2.02 10^{-3}	-2.5

Table 6 – *Identified material parameters – Porcine brain white matter*

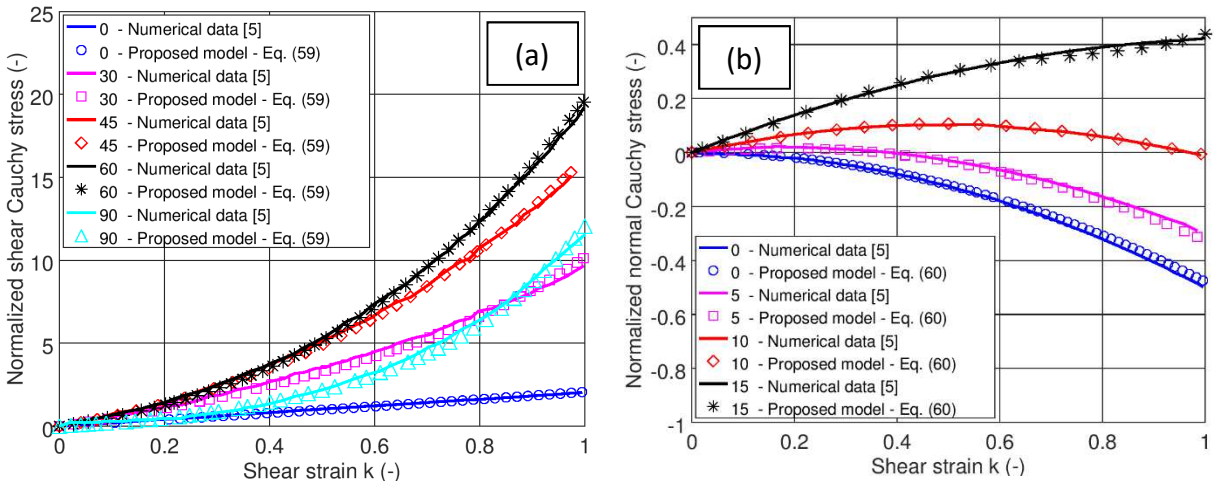

Figure 13 – *Porcine brain white matter – shear (a) and normal (b) stresses normalized by a shear modulus equal to 1.49 kPa*

θ	0°	30°	45°	60°	90°
R^2 σ_{12}/μ	1	0.99	1	1	1
θ	0°	5°	10°	15°	
R^2 σ_{22}/μ	0.99	0.99	0.99	0.99	

Table 7 – *Coefficient of determination* R^2 *for porcine brain white matter*

It is observed in Table 6 that the identified values of the two coefficients $a_2 - a_{24}$ and $a_4 - a_{24}$ are very low compared to the values of the other material parameters. That indicates that these two coefficients likely play a minor role in a shear test. To confirm this guess, we removed these two coefficients from our model and used a model reduced to only

7 parameters: $a_1, a_3, b_3, b_6, b_{24}, \alpha$ and β. By performing a new identification with the shear data extracted from [5], we found the same curves as in Figure 13 and the same coefficients of determination as in Table 7. In the context of a shear loading, it is therefore possible to predict accurately the shear stress with a model containing only 7 material parameters. To understand why the two coefficients $a_2 - a_{24}$ and $a_4 - a_{24}$ were little concerned by a shear test, we considered the linear theory. Particularly, we used equation (19) introduced in [23] to compute the infinitesimal shear modulus μ_L and μ_T (respectively parallel and transverse to the fiber direction) and the infinitesimal longitudinal Young modulus E_L:

$$\mu_T = 2(W_1^0 + W_2^0);\ \mu_L = 2(W_1^0 + W_2^0 + W_5^0) \tag{71}$$

$$E_L = 4(W_{44}^0 + 4W_{45}^0 + 4W_{55}^0) - \mu_T + 4\mu_L \tag{72}$$

In Eq. (71)-(72), the subscripts indicate derivatives with respect to the classical invariants I_1, I_2, I_3, J_4 and J_5:

$$I_1 = Tr(\boldsymbol{C}); I_2 = \frac{1}{2}[I_1^2 - Tr(\boldsymbol{C^2})]; I_3 = det(\boldsymbol{C}); J_4 = Tr(\boldsymbol{Ca} \otimes \mathbf{a}\ ); J_5 = Tr(\boldsymbol{C^2 a} \otimes \mathbf{a}\ ) \tag{73}$$

while the superscript ^{0} denotes evaluation in the reference configuration. In this configuration, the classical invariants reduce to:

$$I_1 = I_2 = 3;\ \ I_3 = 1;\ \ J_4 = J_5 = 1 \tag{74}$$

To calculate W_1^0, we first apply the derivative chain rule to the strain energy function W:

$$W_1 = \omega_1 \frac{\partial K_1}{\partial I_1} + \omega_2 \frac{\partial K_2}{\partial I_1} + \omega_3 \frac{\partial K_3}{\partial I_1} + \omega_4 \frac{\partial K_4}{\partial I_1} + \omega_6 \frac{\partial K_6}{\partial I_1} \tag{75}$$

We next use the link between the invariants K_i and the classical invariants [1]:

$$K_1 = J_4;\ \ K_2 = I_1 - J_4;\ \ K_3 = J_5 - J_4^2;\ \ K_4 = I_1 J_4 - J_5 - I_2;$$

$$K_6 = I_1\ \ (J_5 + J_4^2) - 3J_4 J_5 + J_4^3 + 2I_3 - 2I_2 J_4 \tag{76}$$

The derivatives of the invariants K_i with respect to I_1 are computed straightforwardly from (76):

$$\frac{\partial K_1}{\partial I_1} = \frac{\partial K_3}{\partial I_1} = 0;\ \ \frac{\partial K_2}{\partial I_1} = 1;\ \ \frac{\partial K_4}{\partial I_1} = J_4;\ \ \frac{\partial K_6}{\partial I_1} = J_5 + J_4^2 \tag{77}$$

Reporting Eq. (77) in Eq. (75) yields to:

$$W_1 = \omega_2 + J_4\omega_4 + (J_5 + J_4^2)\omega_6 \tag{78}$$

The three coefficients ω_2, ω_4 and ω_6 are next replaced in Eq. (78) by using Eqs. (21), (23) and (24):

$$W_1 = a_2(K_2 - 2) + b_{24} + a_{24}(K_4 + 1)$$
$$+J_4[a_4(K_4 + 1) + b_{24} + a_{24}(K_2 - 2)] + (J_5 + J_4^2)b_6 \quad (79)$$

To switch from W_1 to W_1^0, Eqs. (19) and (74) are reported in Eq. (79):

$$W_1^0 = 2(b_{24} + b_6) \quad (80)$$

W_2^0, W_5^0, W_{44}^0, W_{45}^0 and W_{55}^0 are calculated the same as W_1^0:

$$W_2^0 = -b_{24} - 2b_6;\ W_5^0 = b_3 - b_{24} \quad (81)$$

$$W_{44}^0 = a_2 + 4a_3 + 9a_4 - 6a_{24} - 2b_3 + 12b_6;\ W_{45}^0 = a_{24} - 2a_3 - 3a_4 - 3b_6;$$
$$W_{55}^0 = a_3 + a_4 \quad (82)$$

The shear modulus μ_L and μ_T are obtained by reporting Eqs. (80) and (81) in Eq. (71):

$$\mu_L = 2b_3;\ \ \mu_T = 2b_{24} \quad (83)$$

Note that it is not inconsistent to find that μ_T is not equal to the initial slope $2b_3 - \alpha$ found in section 4.2 with a shear loading applied transversely to the fiber direction. The explanation comes from the fact that μ_T is calculated from the Cauchy stress $\boldsymbol{\sigma}$ while $2b_3 - \alpha$ is calculated from the nominal stress $\boldsymbol{P}$. Eq. (83) proves that the infinitesimal shear modulus μ_L and μ_T do not depend on the two coefficients $a_2 - a_{24}$ and $a_4 - a_{24}$. Therefore, that makes sense that the three material parameters a_2, a_4 and a_{24} are not concerned by an identification process with a shear test. Finally, the infinitesimal longitudinal Young modulus E_L is obtained by reporting Eqs. (82) and (83) in Eq. (72):

$$E_L = 2\{2(a_2 - a_{24}) + 2(a_4 - a_{24}) - b_{24}\} \quad (84)$$

Contrarily to the shear modulus, the infinitesimal longitudinal Young modulus E_L depend on the two coefficients $a_2 - a_{24}$ and $a_4 - a_{24}$. Therefore, the three material parameters a_2, a_4 and a_{24} must be concerned by an identification process with an extension test. This observation is consistent with the conclusion drawn in section 4.1.

6. Conclusions

In this study, a new strain energy function (SEF) was proposed for modelling incompressible transverse isotropic hyperelastic materials with a single fiber direction. The SEF was built by combining into polynomial and exponential forms the integrity basis of anisotropic invariants proposed in [1]. This combination allows to reach a high level of

regularity with the exponential function and to reduce the number of material parameters from 23 to 10 compared to [2]. In some specific cases, it is possible to reduce more the number of material parameters and get a simpler version of the model. For example, if one is only interested in a tensile test, it is possible to reduce the number of material parameters from 10 to 5 as explained in section 4.1. Moreover, it is proved in section 5.4 that performing an identification process based on shear experiments only require 7 of the 10 material parameters of our model. However, in the most complicated loading case mixing tensile and shear tests, the use of the 10 material parameters embedded in our model is required.

In order to identify the 10 material parameters of the proposed model, we have developed and implemented specific original optimization tools inside the Octave free software because we have to cope with a wide variety of loading cases: uniaxial tension and shear tests, both parallel and transverse to the fiber direction [3, 4], as well as shear tests with 9 different fiber angles [5]. The non-standard identification strategies we have implemented are based on: 1) the linear or nonlinear nature of the material parameters; 2) the modeling of the free boundary conditions by a spectral approach.

Finally, we compared our model with experimental and numerical data extracted from the literature [3-5]. These comparisons, which relate to various loading cases and materials, demonstrate that our model is capable to accurately predict the mechanical behavior of one-fiber anisotropic hyperelastic structures.

Acknowledgements

This work was supported by the National Key R&D Program of China [grant number 2017YFB0703200], the National Natural Science Foundation of China [grant number 11772274], Guangdong New Energy Vehicle Power and Safety System Engineering Technology Research Center, the Science and Technology Planning Projects of Guangzhou, China [grant number 201803030041] and the Science and Technology Planning Projects of Guangzhou, China [grant number 201905010007].

References

[1] AT Ta, F Holweck, N Labed, A Thionnet, F Peyraut. A constructive approach of invariants

of behavior laws with respect to an infinite symmetry group–application to a biological anisotropic hyperelastic material with one fiber family. International Journal of Solids and Structures, 51(21):3579–3588, 2014.

[2] RY Cai, F Holweck, ZQ Feng, F Peyraut. A new hyperelastic model for anisotropic hyperelastic materials with one fiber family. International Journal of Solids and Structures, 84:1–16, 2016.

[3] P Ciarletta, I Izzo, S Micera, F Tendick. Stiffening by fiber reinforcement in soft materials: a hyperelastic theory at large strains and its application. Journal of the Mechanical Behavior of Biomedical Materials, 4(7):1359–1368, 2011.

[4] FM Davis, R De Vita. A three-dimensional constitutive model for the stress relaxation of articular ligaments. Biomech Model Mechanobiol, 13: 653–663, 2014.

[5] CO Horgan, JG Murphy. Fiber orientation effects in simple shearing of fibrous soft tissues. Journal of Biomechanics, 64: 131–135, 2017.

[6] F Goulette, ZW Chen. Fast computation of soft tissue deformations in real-time simulation with hyper-elastic mass links. Computer Methods in Applied Mechanics and Engineering, 295:18–38, 2015.

[7] TC Gasser, RW Ogden, GA Holzapfel. Hyperelastic modelling of arterial layers with distributed collagen fibre orientations. Journal of the Royal Society Interface, 3(6):15–35, 2006.

[8] GA Holzapfel, TC Gasser, RW Ogden. A new constitutive framework for arterial wall mechanics and a comparative study of material models. Journal of elasticity and the Physical Science of Solids, 61(1-3):1–48, 2000.

[9] T Shearer. A new strain energy function for the hyperelastic modelling of ligaments and tendons based on fascicle microstructure. Journal of Biomechanics, 48(2):290–297, 2015.

[10] G Limbert, J Middleton. A constitutive model of the posterior cruciate ligament. Medical Engineering & Physics, 28(2):99–113, 2006.

[11] B Fereidoonnezhad, R Naghdabadi, J Arghavani. A hyperelastic constitutive model for fiber-reinforced rubber-like materials. International Journal of Engineering Science, 71:36–44, 2013.

[12] JA Weiss, BN Maker, S Govindjee. Finite element implementation of incompressible, transversely isotropic hyperelasticity. Computer Methods in Applied Mechanics and Engineering, 135(1):107–128, 1996.

[13] D Balzani, P Neff, J Schroder, GA Holzapfel. A polyconvex framework for soft biological tissues. adjustment to experimental data. International Journal of Solids and Structures, 43(20):6052–6070, 2006.

[14] DJ O'Shea, MM Attard, DC Kellermann. Hyperelastic constitutive modelling for transversely isotropic composites and orthotropic biological tissues. International Journal of Solids and Structures, 169, 1–20, 2019.

[15] A Thionnet, C Martin. A new constructive method using the theory of invariants to obtain material behavior laws. International Journal of Solids and Structures, 43(2):325–345, 2006.

[16] JW Eaton, D Bateman, S Hauberg, R Wehbring. GNU Octave version 4.2.0 manual: a high-level interactive language for numerical computations, 2016.

[17] Y Lanir, YC Fung. Two-dimensional mechanical properties of rabbit skin-ii. experimental results. Journal of Biomechanics, 7(2):171–182, 1974.

[18] P Tong, YC Fung. The stress-strain relationship for the skin. Journal of Biomechanics, 9(10):649–657, 1976.

[19] N Harb, N Labed, M Domaszewski, F Peyraut. A new parameter identification method of soft biological tissue combining genetic algorithm with analytical optimization. Computer Methods in Applied Mechanics and Engineering, 200(1-4):208-215, 2011.

[20] A. Kossa, S. Berezvai. Novel strategy for the hyperelastic parameter fitting procedure of polymer foam materials. Polymer Testing, 53:149-155, 2016.

[21] KM Quapp, JA Weiss. Material characterization of human medial collateral ligament. Journal of Biomechanical Engineering, 120 (6):757-763, 1998.

[22] Y Feng, C.-H Lee, L Sun, S Ji, X Zhao. Characterizing white matter tissue in large strain via asymmetric indentation and inverse finite element modeling. Journal of the Mechanical Behavior of Biomedical Materials, 65: 490–501, 2017.

[23] J.G. Murphy. Transversely isotropic biological, soft tissue must be modelled using both anisotropic invariants. European Journal of Mechanics A/Solids, 42, 90–96, 2013.

[24] G.Y. Qiu, T.J. Pence. Remarks on the behavior of simple directionally reinforced incompressible nonlinearly elastic solids. Journal of Elasticity, 49, 1–30, 1997.

[25] J. Merodio, R.W. Ogden. Mechanical response of fiber-reinforced incompressible non-linearly elastic solids. International Journal of Non-Linear Mechanics, 40, 213–227, 2005.

[26] Z.Y., Guo, X.Q. Peng, B. Moran. Mechanical response of neo-Hookean fiber reinforced incompressible nonlinearly elastic solids. International Journal of Solids and Structures, 44, 1949–1969, 2007.